Proceedings of the Indian National Science Academy (2026) 92:586–598
https://doi.org/10.1007/s43538-025-00429-8

RESEARCH PAPER

Investigating dynamics of fiber metal laminate plates exposed to time-dependent uniform pressure loading

Jin Lin[1]

Received: 24 July 2024 / Accepted: 31 March 2025 / Published online: 25 April 2025

Abstract
Fiber metal laminates find widespread applications in various industries, including aerospace, marine, automotive, and pressure vessel manufacturing. This study focuses on analytically investigating the behavior of fiber-metal-laminate exposed to time dependent pressure loading. To achieve this, the laminates are modeled using Reddy's higher-order shear deformation theory, incorporating von Karman's geometric nonlinear effects in derivation of equations of motion. The laminates are supposed to be situated on a Pasternak substrate, with boundary conditions set as simple supports along all plate edges. The motion equations, characterized by nonlinear partial derivatives, are discretized using Galerkin technique and subsequently resolved via Runge–Kutta technique. The obtained results are compared with those from previous studies, demonstrating favorable agreement. Furthermore, the study explores the influence of several key parameters, including aspect ratio, Pasternak substrate characteristics, loading duration, and pressure pulse type, on vibration response of laminates. The findings indicate that reducing the duration of the positive loading phase while increasing the wave function amplifies the impact of the negative loading phase, leading to increase dimensionless displacement at the plate center. Additionally, it is observed that the shear layer constraint has a more pronounced influence on the time response compared to the linear stiffness parameter.

Keywords Nonlinear dynamic · Fiber-metal laminate · Higher-order shear deformation theory · Blast loading

Introduction

In recent decades, reducing the weight of aerospace structures has become very important due to the lessening of fuel consumption and the prevention of cost wastage and the spread of carbon dioxide in space. To achieve this goal, due to the weak points of metals, composites, and fiber metal laminates were widely used in aerospace structures (Ma et al. 2023; Ng et al. 2023; Costa et al. 2023; Niu et al. 2023). Metals and composites each have their advantages and disadvantages. Metals have disadvantages such as high mass density, relatively low corrosion resistance, and low fatigue resistance, while composites have disadvantages such as low impact tolerance and energy absorption, low residual strength after impact, and low reparability. Disadvantages in metals and composites can be improved by combining them into fiber metal laminates (Smolnicki et al. 2023). Among the applications of fiber metal laminates are interior panels of aircraft, aircraft brakes, sports equipment, sea vessels, medical equipment, railway wagons, trains, and other applications (Xie et al. 2024). Fiber metal laminates, according to the type of fibers used in the polymer matrix, are divided into three types of laminates reinforced with aramid fibers, glass fibers, and carbon fibers (Blala et al. 2021).

Fiber-metal-laminates (FMLs) are hybrid materials that combine the lightweight and high-strength properties of metal layers with the stiffness and fatigue resistance of fiber-reinforced polymer layers. These materials are extensively used in various engineering fields, including automotive, aerospace, and marine industries, due to their excellent mechanical properties, impact resistance, and structural reliability. Numerous studies have been conducted to analyze the dynamic and static behaviors of many structures under different loading and environmental conditions (Chen et al. 2023; Lu 2024; Samuel and Adewunmi 2024; Flayyih and Hassan 2024). Recent research has expanded to include smart FML plates, where piezoelectric materials or shape memory alloys are embedded within the laminate

✉ Jin Lin
linjin_wx@126.com

1 Intelligent manufacturing Automotive Engineering College, Wuxi Vocational Institute of Commerce, Wuxi 214153, Jiangsu, China

structure to enhance functionality, such as vibration control, self-healing, or structural health monitoring (Wang et al. 2023). These studies highlight the potential of smart FMLs in adaptive and multifunctional structures, addressing challenges in real-time response and durability (Gurbanov et al. 2020). For example, investigations into smart FMLs under dynamic loading have demonstrated improvements in vibration suppression and damage detection capabilities, making them suitable for advanced aerospace applications (Etri et al. 2022). Another critical area of research involves impact loading on FML plates, where the focus is on understanding the response to high-velocity impacts, such as bird strikes or ballistic impacts, as well as low-velocity impacts, including tool drops or hail (Kakati and Chakraborty 2023). These studies employ experimental, numerical, and analytical methods to evaluate parameters such as energy absorption, delamination, and residual strength. Insights from these works have been instrumental in optimizing FML design for applications requiring high impact resistance and fatigue life.

The dynamics of isotropic beams (Shabani et al. 2013; Rezaee and Sharafkhani 2019), plates (Ebrahimi-Mamaghani et al. 2023, 2024; Ebrahimi et al. 2013) and composite multilayers have been widely studied in recent years (Sharafkhani et al. 2022; Gharebagh et al. 2011; Madinei et al. 2013). Zhao et al. (2023) proposed a 3D elasticity response for free dynamics of plates with some different boundary conditions. Zhen et al. (2021) studied the free dynamics of square thick composites via the third-order shear theory and numerical technique. In another research, Van Do and Lee (2021) presented a non-uniform rational B-spline using the 3rd-order Reddy's theory and using it examined the static response and vibrations of square-shaped composites. Ahmadi et al. (2017) investigated the buckling, bending, and free vibrations of composites reinforced with carbon nanotubes having different geometrical shapes using a multi-scale numerical modeling method. Lim et al. (2013) proposed an analytical method to study the nonlinear dynamics of sandwich plates. The governing differential equations of motion were derived using higher-order shear deformation theory in conjunction with Hamilton's principle. These equations were solved using Navier's solution method and the Runge–Kutta technique. The interlaminar stresses are achieved through the sandwich plate thickness. Rezaee et al. (2025) investigated the dynamic response of viscoelastic beams subjected to fluid stimulation, focusing on nonlinear effects and uncertainties. Pourreza et al. (2025) analyzed the nonlinear vibrations of cracked graphene nanoplates in a magnetic field using nonlocal elasticity. These studies showcase advanced modeling techniques for understanding dynamic behavior in complex systems at macro and nanoscale.

Also, several researchers have studied the nonlinear vibrations of composites using numerical and semi-analytical methods. Keshavarzian et al. (2022) investigated nonlinear in-plane dynamics for plates via the perturbation theory. Szekrenyes (2021) based on Reddy's theory, presented the equations governing the nonlinear vibrations of orthotropic plates with limited deformations. They investigated free nonlinear vibrations using the DQM. Maraş and Yaman (2022) studied linear and nonlinear dynamics of rectangular fiber metal laminates by 1st-order shear theory. To achieve the nonlinear response, they used the multiple scales method and investigated the structure of nonlinear frequencies. Shooshtari and Razavi (2010) used the least squares-based finite difference technique to solve large-amplitude free dynamics problems for plates with arbitrary geometric shapes. Amabili et al. (2020) considered the nonlinear response of laminate plates and cylinders under blast loading using the numerical technique and the Tsai-Wu criterion. Also, Dinh Duc et al. (2017) examined the nonlinear dynamics of the plate made of functionally graded metal-ceramic materials exposed to blast and thermal loading using higher-order theory. Patel et al. (2023) evaluated the geometric nonlinear dynamics of FML cylindrical shells under blast loading with various boundary conditions using numerical simulations. As can be seen, many studies have been conducted on the natural frequency and dynamics of plates with different boundary conditions and loads.

While extensive research has been conducted on the nonlinear dynamic response of composite laminates, as discussed in Reference (Upadhyay et al. 2011), this study focuses on FMLs, a unique class of hybrid materials combining metal and fiber-reinforced polymer layers. FMLs exhibit distinct mechanical properties, such as improved impact resistance, enhanced energy absorption, and superior fatigue behavior, which differ significantly from those of conventional composite laminates. These characteristics necessitate a tailored analysis to accurately capture their dynamic response under various loading conditions.

According to the conducted research, investigating the performance of fiber-metal composite laminates under time loadings, especially blast wave loading, has generally been conducted experimentally or by using finite element simulations with commercial codes. Also, most of the studies have been accomplished using higher-order theories considering the strains to be linear. Therefore, in the present research, for the first time, using Reddy's theory, taking into account von Karman's nonlinear strains, the response of FML under time-dependent uniform pressure forces has been investigated. The boundary conditions of the plate at all edges are considered simple supports, and it is assumed that the fiber metal laminate is placed on the Pasternak substrate. According to the Hamilton principle, displacement terms are used to obtain the problem's governing structural equations.

The Runge–Kutta numerical technique is then used to solve nonlinear equations once the equations have been discretized using the Galerkin technique. The analytical results are compared with the results existing in previous studies. Also, in order to examine the effect of parameters governing the problem, the impact of ratio, Pasternak substrate, loading time, and kind of pressure pulses (triangular, step, and uniform exponential blast waveforms) on the dynamics of FML has been investigated.

Governing equations

As seen in Fig. 1, an FML plate, which is composed of aluminum and composite layers, having length a, thickness h, and width b, is placed on a Pasternak substrate consisting of linear and shear springs. In addition, it has been supposed that the structure is exposed to a uniform load varying with time P_t in different triangular, step, and exponential blast waveforms. The plate displacement field has been modeled in this study using the third-order shear theory. The requirement that there be no transverse shear stress on the external surfaces is likewise met by this theory. The stress is parabolically changed along the thickness, and the theory can take into account the distortion created in the deformed state when the plate is bent.

In accordance with the third-order shear deformation theory, the displacement field can be expressed as follows:

$$u(x,y,z,t) = u_0(x,y,t) + z\theta_x(x,y,t) - \frac{4z^3}{3h^2}\left(\theta_x(x,y,t) + \frac{\partial w_0(x,y,t)}{\partial x}\right) \tag{1a}$$

$$v(x,y,z,t) = v_0(x,y,t) + z\theta_y(x,y,t) - \frac{4z^3}{3h^2}\left(\theta_y(x,y,t) + \frac{\partial w_0(x,y,t)}{\partial y}\right) \tag{1b}$$

$$w(x,y,z,t) = w_0(x,y,t) \tag{1c}$$

in which θ_x and θ_y are rotations of the transverse plane perpendicular to the x and y axes.

In this study, it is assumed that the structure has large deformation and small strain. For this purpose, Karman's theory is used to express strain–displacement relationships, while if a large strain is assumed, the finite strain technique can be applied to model the strain–displacement (Minaei et al. 2021; Pourreza et al. 2022; Nasrabadi et al. 2022; Hoseinzadeh et al. 2023). According to von Karman's theory of nonlinear strains, strain–displacement relations will be in the form of Eqs. (2a–e) (Pourreza et al. 2021). In Eqs. (2a–e), $\varepsilon_{xx}, \varepsilon_{yy}, \gamma_{xy}, \gamma_{xz}, \gamma$ there are engineering strains. Since the FML laminate consists of composite layers with different fiber angles, the mechanical properties of each layer must be transferred to the coordinates on the axis. Based on the plane stress state, using Hook's model, the stress–strain structural relations for each layer with different fiber angles are expressed as Eq. (3).

$$\varepsilon_{xx} = \frac{\partial u_0}{\partial x} + \frac{1}{2}\left(\frac{\partial w_0}{\partial x}\right)^2 + z\frac{\partial \theta_x}{\partial x} - \frac{4z^3}{3h^2}\left(\frac{\partial \theta_x}{\partial x} + \frac{\partial^2 w_0}{\partial x^2}\right) \tag{2a}$$

$$\varepsilon_{yy} = \frac{\partial v_0}{\partial y} + \frac{1}{2}\left(\frac{\partial w_0}{\partial y}\right)^2 + z\frac{\partial \theta_y}{\partial y} - \frac{4z^3}{3h^2}\left(\frac{\partial \theta_y}{\partial y} + \frac{\partial^2 w_0}{\partial y^2}\right) \tag{2b}$$

$$\gamma_{xz} = \theta_x + \frac{\partial w_0}{\partial x} - \frac{4}{h^2}z^2\left(\theta_x + \frac{\partial w_0}{\partial x}\right) \tag{2c}$$

$$\gamma_{yz} = \theta_y + \frac{\partial w_0}{\partial y} - \frac{4}{h^2}z^2\left(\theta_y + \frac{\partial w_0}{\partial y}\right) \tag{2d}$$

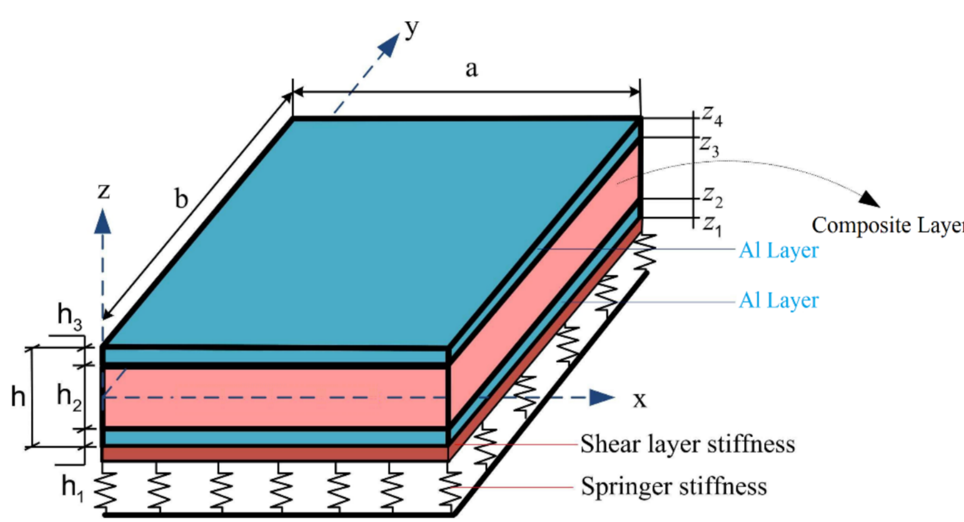

Fig. 1 Fiber metal laminate under dynamic load

$$\gamma_{xy} = \frac{\partial u_0}{\partial y} + \frac{\partial v_0}{\partial x} + \frac{\partial w_0}{\partial x}\frac{\partial w_0}{\partial y} + z\left(\frac{\partial \theta_x}{\partial y} + \frac{\partial \theta_y}{\partial x}\right) - \frac{4z^3}{3h^2}\left(\frac{\partial \theta_x}{\partial y} + \frac{\partial \theta_y}{\partial x} + 2\frac{\partial^2 w_0}{\partial x \partial x}\right) \tag{2e}$$

$$\begin{bmatrix} \sigma_{xx} \\ \sigma_{yy} \\ \sigma_{xy} \\ \sigma_{yz} \\ \sigma_{xz} \end{bmatrix}_k = \begin{bmatrix} \overline{Q}_{1-1} & \overline{Q}_{1-2} & \overline{Q}_{1-6} & 0 & 0 \\ \overline{Q}_{2-1} & \overline{Q}_{2-2} & \overline{Q}_{2-6} & 0 & 0 \\ \overline{Q}_{6-1} & \overline{Q}_{6-2} & \overline{Q}_{6-6} & 0 & 0 \\ 0 & 0 & 0 & \overline{Q}_{4-4} & \overline{Q}_{4-5} \\ 0 & 0 & 0 & \overline{Q}_{5-4} & \overline{Q}_{5-5} \end{bmatrix}_k \begin{bmatrix} \varepsilon_{xx} \\ \varepsilon_{yy} \\ \gamma_{xy} \\ \gamma_{yz} \\ \gamma_{xz} \end{bmatrix}_k \tag{3}$$

in which Q_{ij} remains the reduced stiffness constants for the kth layer. For composite materials, the reduced stiffness constants are determined based on the fiber orientation within the laminate. These stiffness constants, which govern the mechanical behavior of each layer, are calculated using standard transformation equations widely available in the literature. These equations account for the elastic properties of constituent materials and angle of the fibers within each composite layer (Reddy 2003).

According to Eq. (3), the constants $\overline{Q}_{16}, \overline{Q}_{26}, \overline{Q}_{45}$, in cross-fiber composites will be zero. In the above relation Q_{ij}, the constants are:

$$Q_{11} = \frac{E_1}{1 - \vartheta_{12}\vartheta_{21}}, Q_{22} = \frac{E_2}{1 - \vartheta_{12}\vartheta_{21}}, Q_{12} = \frac{\vartheta_{12}E_2}{1 - \vartheta_{12}\vartheta_{21}}, \quad Q_{66} = G_{12}, Q_{44} = G_{23}, Q_{55} = G_{13} \tag{4}$$

The equations governing of system motion are derived via the Hamilton's principle, which provides a variational framework for obtaining the equations of motion. This principle states that the true dynamic path of a system corresponds to the stationary value of the action integral, formulated based on the difference between kinetic and potential energies and work done by external forces as (Hwang and Park 1993):

$$\delta \int_0^t (U - T + W)dt = 0 \tag{5}$$

where T is the kinetic energy, U the potential energy, and W the work done by the external forces. Variation of kinetic energy expressed as follows:

$$\begin{aligned}
\delta T = \iint \Bigg[& I_0\left(\frac{\partial u_0}{\partial t}\delta\frac{\partial u_0}{\partial t} + \frac{\partial v_0}{\partial t}\delta\frac{\partial v_0}{\partial t} + \frac{\partial w_0}{\partial t}\delta\frac{\partial w_0}{\partial t}\right) \\
& + I_1\left(\frac{\partial u_0}{\partial t}\delta\frac{\partial \theta_x}{\partial t} + \frac{\partial v_0}{\partial t}\delta\frac{\partial \theta_y}{\partial t} + \frac{\partial w_0}{\partial t}\delta\frac{\partial \theta_z}{\partial t}\right) \\
& + I_2\left(\frac{\partial \theta_x}{\partial t}\frac{\partial \delta\theta_x}{\partial t} + \frac{\partial \theta_y}{\partial t}\frac{\partial \delta\theta_y}{\partial t}\right) \\
& - I_3C_1\left(\frac{\partial u_0}{\partial t}\frac{\partial \delta\theta_x}{\partial t} + \frac{\partial v_0}{\partial t}\frac{\partial \delta\theta_y}{\partial t} + \frac{\partial u_0}{\partial t}\frac{\partial^2 \delta w_0}{\partial x \partial t} + \frac{\partial v_0}{\partial t}\frac{\partial^2 \delta w_0}{\partial y \partial t} + \frac{\partial \theta_x}{\partial t}\frac{\partial \delta u_0}{\partial t} + \frac{\partial \theta_y}{\partial t}\frac{\partial \delta v_0}{\partial t} + \frac{\partial \delta u_0}{\partial t}\frac{\partial^2 w_0}{\partial x \partial t} + \frac{\partial \delta v_0}{\partial t}\frac{\partial^2 w_0}{\partial y \partial t}\right) \\
& - I_4C_1\left(\frac{\partial \theta_x}{\partial t}\frac{\partial^2 \delta w_0}{\partial x \partial t} + \frac{\partial \theta_y}{\partial t}\frac{\partial^2 \delta w_0}{\partial y \partial t} + 2\left(\frac{\partial \theta_x}{\partial t}\frac{\partial \delta\theta_x}{\partial t} + \frac{\partial \theta_y}{\partial t}\frac{\partial \delta\theta_y}{\partial t}\right) + \frac{\partial \delta\theta_y}{\partial t}\frac{\partial^2 w_0}{\partial x \partial t} + \frac{\partial \delta\theta_y}{\partial t}\frac{\partial^2 w_0}{\partial y \partial t}\right) \\
& + I_6C_1^2\left(\frac{\partial \theta_x}{\partial t}\frac{\partial \delta\theta_x}{\partial t} + \frac{\partial \theta_y}{\partial t}\frac{\partial \delta\theta_y}{\partial t} + \frac{\partial \theta_x}{\partial t}\frac{\partial^2 \delta w_0}{\partial x \partial t} + \frac{\partial \theta_y}{\partial t}\frac{\partial^2 \delta w_0}{\partial y \partial t} + \frac{\partial \delta\theta_x}{\partial t}\frac{\partial^2 w_0}{\partial x \partial t} + \frac{\partial^2 w_0}{\partial y \partial t}\frac{\partial \delta\theta_y}{\partial t} + \frac{\partial^2 \delta w_0}{\partial x \partial t}\frac{\partial^2 w_0}{\partial x \partial t} + \frac{\partial^2 w_0}{\partial y \partial t}\frac{\partial^2 \delta w_0}{\partial y \partial t}\right)\Bigg] dA
\end{aligned} \tag{6}$$

in which $C_1 = 4/3h^2$, mass inertia parameters I_6, I_4, I_2, I_1, I are also expressed as follows:

$$I_j = \int_{-h/2}^{+h/2} \rho^j dz \ and \ j = 0, 1, ..., 6 \tag{7}$$

Also, the strain energy term is in the form of Eq. (8):

$$\delta U = \int \left(\sigma_{xx}\delta\varepsilon_{xx} + \sigma_{yy}\delta\varepsilon_{yy} + \sigma_{xy}\delta\gamma_{xy} + \sigma_{xz}\delta\gamma_{xz} + \sigma_{yz}\delta\gamma_{yz}\right)$$

$$\begin{aligned} dV = \int \Bigg\{ & N_{xx}\delta\left(\frac{\partial u_0}{\partial x} + \frac{1}{2}\left(\frac{\partial w_0}{\partial x}\right)^2\right) - C_1P_{xx}\delta\left(\frac{\partial \theta_x}{\partial x} + \frac{\partial^2 w_0}{\partial x^2}\right) + N_{yy}\delta\left(\frac{\partial v_0}{\partial y} + \frac{1}{2}\left(\frac{\partial w_0}{\partial y}\right)^2\right) \\ & + M_{xx}\delta\frac{\partial \theta_x}{\partial x} + N_{xy}\delta\left(\frac{\partial u_0}{\partial y} + \frac{\partial v_0}{\partial x} + \frac{\partial w_0}{\partial x}\frac{\partial w_0}{\partial y}\right) + M_{yy}\delta\frac{\partial \theta_y}{\partial y} - P_{xy}C_1\delta\left(\frac{\partial \theta_x}{\partial y} + \frac{\partial \theta_y}{\partial x} + 2\frac{\partial^2 w_0}{\partial x}\right) \\ & M_{xy}\delta\left(\frac{\partial \theta_x}{\partial y} + \frac{\partial \theta_y}{\partial x}\right) - C_1P_{yy}\delta\left(\frac{\partial \theta_y}{\partial y} + \frac{\partial^2 w_0}{\partial y^2}\right) + +Q_{xz}\delta\left(\theta_x + \frac{\partial w_0}{\partial x}\right) \\ & - 3C_1R_{xz}\delta\left(\theta_x + \frac{\partial w_0}{\partial x}\right) + Q_{yz}\delta\left(\theta_y + \frac{\partial w_0}{\partial y}\right) - 3C_1R_{yz}\delta\left(\theta_y + \frac{\partial w_0}{\partial y}\right)\Bigg\} dA \end{aligned} \tag{8}$$

in which the parameters N_{ij}, M_{ij}, P_{ij}, Q_{ij} and R_{ij} are:

$$\{N_{xx}, N_{xy}, N_{yy}\} = \int_{-\frac{h}{2}}^{\frac{h}{2}} \{\sigma_{xx}, \sigma_{xy}, \sigma_{yy}\} dz \tag{9a}$$

$$\{M_{xx}, M_{xy}, M_{yy}\} = \int_{-\frac{h}{2}}^{\frac{h}{2}} \{\sigma_{xx}, \sigma_{xy}, \sigma_{yy}\} z dz \tag{9b}$$

$$\{P_{xx}, P_{xy}, P_{yy}\} = \int_{-\frac{h}{2}}^{\frac{h}{2}} \{\sigma_{xx}, \sigma_{xy}, \sigma_{yy}\} z^3 dz \tag{10a}$$

$$\{P_{xz}, P_{yz}\} = \int_{-\frac{h}{2}}^{\frac{h}{2}} \{\sigma_{xz}, \sigma_{yz}\} dz \tag{10b}$$

$$\{R_{xz}, R_{yz}\} = \int_{-\frac{h}{2}}^{\frac{h}{2}} \{\sigma_{xz}, \sigma_{yz}\} z^2 dz \tag{10c}$$

The term related to the energy changes caused by the external forces work due to the application of time-varying loading as well as the energy changes caused by the Pasternak substrate is expressed as follows, where *q(t)* is the load of step force or triangular load:

$$\delta V = \int \left\{ q(t) + k_p\left(\frac{\partial^2 w_0}{\partial x^2} + \frac{\partial^2 w_0}{\partial y^2}\right) + k_e w_0 \right\} \partial w_0 \tag{11}$$

Finally, by using Eqs. (6), (8), and (11) and placing them into the relation of Hamilton's principle as well as using the method of integration by parts to simplify the terms, the equations governing the movement of the system are extracted as:

$$\delta u_0 : \frac{\partial N_{xx}}{\partial x} + \frac{\partial N_{xy}}{\partial y} = I_0\frac{\partial^2 u_0}{\partial t^2} + I_1\frac{\partial^2 \theta_x}{\partial t^2} - I_3C_1\frac{\partial^2 \theta_x}{\partial t^2} - I_3C_1\frac{\partial^3 w_0}{\partial x \partial t^2} \tag{12a}$$

$$\delta v_0 : \frac{\partial N_{yy}}{\partial y} + \frac{\partial N_{xy}}{\partial x} = I_0\frac{\partial^2 v_0}{\partial t^2} + I_1\frac{\partial^2 \theta_y}{\partial t^2} - I_3C_1\frac{\partial^2 \theta_y}{\partial t^2} - I_3C_1\frac{\partial^3 w_0}{\partial y \partial t^2} \tag{12b}$$

$$\begin{aligned} \delta w_0 : \; & N_{xx}\frac{\partial^2 w_0}{\partial x^2} + \frac{\partial N_{xx}}{\partial x}\frac{\partial w_0}{\partial x} + C_1\frac{\partial^2 P_{xx}}{\partial x^2} + N_{yy}\frac{\partial^2 w_0}{\partial y^2} \\ & + \frac{\partial N_{yy}}{\partial y}\frac{\partial w_0}{\partial y} + C_1\frac{\partial^2 P_{yy}}{\partial y^2} + 2N_{xy}\frac{\partial^2 w_0}{\partial x \partial y} + \frac{\partial N_{xy}}{\partial y}\frac{\partial w_0}{\partial x} \\ & + \frac{\partial N_{xy}}{\partial x}\frac{\partial w_0}{\partial y} + 2C_1\frac{\partial^2 P_{xy}}{\partial x \partial y} + \frac{\partial Q_{xz}}{\partial x} \\ & - 3C_1\frac{\partial R_{xz}}{\partial x} + \frac{\partial Q_{yz}}{\partial y} - 3C_1\frac{\partial R_{yz}}{\partial y} + K_e w_0 \\ & + K_p\left(\frac{\partial^2 w_0}{\partial x^2} + \frac{\partial^2 w_0}{\partial y^2}\right) + q = I_0\frac{\partial^2 w_0}{\partial t^2} + I_3C_1\frac{\partial^3 u_0}{\partial x \partial t^2} \\ & + I_3C_1\frac{\partial^3 v_0}{\partial y \partial t^2} + I_4C_1\frac{\partial^3 \theta_x}{\partial x \partial t^2} + I_4C_1\frac{\partial^3 \theta_y}{\partial y \partial t^2} \\ & - I_6C_1^2\left(\frac{\partial^3 \theta_x}{\partial x \partial t^2} + \frac{\partial^3 \theta_y}{\partial y \partial t^2}\right) \end{aligned} \tag{12c}$$

$$\begin{aligned} \delta \theta_x : \; & \frac{\partial M_{xx}}{\partial x} - C_1\frac{\partial P_{xx}}{\partial x} + \frac{\partial M_{xy}}{\partial y} - C_1\frac{\partial P_{xy}}{\partial y} - Q_{xz} \\ & + 3C_1R_{xz} = I_1\frac{\partial^2 u_0}{\partial t^2} + I_2\frac{\partial^2 \theta_x}{\partial t^2} - I_3C_1\frac{\partial^2 u_0}{\partial t^2} \\ & - 2I_4C_1\frac{\partial^2 \theta_x}{\partial t^2} - I_4C_1\frac{\partial^3 w_0}{\partial x \partial t^2} + I_6{C_1}^2\frac{\partial^2 \theta_x}{\partial t^2} + I_6{C_1}^2\frac{\partial^3 w_0}{\partial x \partial t^2} \end{aligned} \tag{12d}$$

$$\delta\theta_y : \frac{\partial M_{yy}}{\partial y} - C_1\frac{\partial P_{yy}}{\partial y} + \frac{\partial M_{xy}}{\partial x} - C_1\frac{\partial P_{xy}}{\partial x} - Q_{yz} + 3C_1R_{yz} = I_1\frac{\partial^2 v_0}{\partial t^2} + I_2\frac{\partial^2 \theta_y}{\partial t^2} - I_3C_1\frac{\partial^2 v_0}{\partial t^2} - 2I_4C_1\frac{\partial^2 \theta_y}{\partial t^2} - I_4C_1\frac{\partial^3 w_0}{\partial y\partial t^2} + I_6C_1^2\frac{\partial^2 \theta_y}{\partial t^2} + I_6C_1^2\frac{\partial^3 w_0}{\partial y\partial t^2} \tag{12e}$$

Using Eqs. (10a–c) and (12a–e), the general equations governing the problem will be obtained in terms of displacement fields.

Dynamic loading

Advanced supersonic and hypersonic flying devices are subjected to a variety of dynamic loads such as gusts, shock loads, intense sound pulses, and blast waves. The analysis and design of structures under dynamic loading such as blast waves requires a detailed understanding of the loading phenomenon. Therefore, in the present research, the effects of different types of time-dependent pressure pulses have been investigated. The types of the loads and their functions are as follows:

Triangular loading

$$R(t) = \begin{cases} \left(1 - \frac{t}{t_1}\right)Q_0, & \text{for} \quad t \le t_1 \\ 0 & \text{for} \quad t > t_1 \end{cases} \tag{13}$$

Uniform blast loading

The Friedländer function is an ideal laboratory function for the pressure–time curve of the blast wave caused by an explosion in open air, which reaches a point with a safe distance from the explosion point. If the resulting loading can be assumed to be uniform, the resulting wave can be considered as an exponential shape function called the Friedländer function (Dobyns 1981):

$$R(t) = \begin{cases} Q_0 e^{-\alpha\frac{t}{t_1}}\left(1 - \frac{t}{t_1}\right), & \text{for} \quad t \le t_1 \\ 0 & \text{for} \quad t > t_1 \end{cases} \tag{14}$$

Step loading

$$q(t) = Q_0 \tag{15}$$

In Eqs. (13) to (15), the constants Q_0, t_1, and a are the maximum blast pressure, duration of the positive phase of loading, and the wave function, respectively.

Solution method

For the edges of the FML, simply supported boundary conditions are considered. Therefore, the displacement and moment around the panel are zero. As a result, the boundary conditions will be as follows:

$$\begin{aligned} &u_0(x,0,t) = v_0(a,y,t) = u_0(x,b,t) = v_0(0,y,t) = 0 \\ &w_0(x,0,t) = w_0(x,b,t) = w_0(0,y,t) = w_0(a,y,t) = 0 \\ &\theta_x(x,0,t) = \theta_x(x,b,t) = \theta_y(0,y,t) = \theta_y(a,y,t) = 0 \\ &M_{xx}(0,y,t) = M_{yy}(x,0,t) = M_{xx}(a,y,t) = M_{yy}(x,b,t) = 0 \\ &P_{xx}(0,y,t) = P_{yy}(x,0,t) = P_{xx}(a,y,t) = P_{yy}(x,b,t) = 0 \end{aligned} \tag{16}$$

In the Galerkin technique, the trial functions are selected to satisfy the geometric boundary conditions, such as displacement and slope constraints, while the force boundary conditions are handled indirectly through the variational formulation. The stresses derived from the displacement fields are validated against the force boundary conditions, ensuring that they are satisfied in an approximate sense. This approach is consistent with standard practices in structural mechanics and has been validated through convergence studies and comparison with benchmark results (Rao 2019; Rezaee and Maleki 2024). According to the governing boundary conditions, the proposed Fourier series for displacement fields are considered as:

$$\begin{aligned} &u_0(x,y,t) = \sum_{m=1}^{M}\sum_{n=1}^{N}\cos\left(\frac{m\pi x}{a}\right)\sin\left(\frac{n\pi y}{b}\right)U_{mn}(t) \\ &v_0(x,y,t) = \sum_{m=1}^{M}\sum_{n=1}^{N}\sin\left(\frac{m\pi x}{a}\right)\cos\left(\frac{n\pi y}{b}\right)V_{mn}(t) \\ &W_0(x,y,t) = \sum_{m=1}^{M}\sum_{n=1}^{N}\sin\left(\frac{m\pi x}{a}\right)\sin\left(\frac{n\pi y}{b}\right)W_{mn}(t) \\ &\theta_x(x,y,t) = \sum_{m=1}^{M}\sum_{n=1}^{N}\cos\left(\frac{m\pi x}{a}\right)\sin\left(\frac{n\pi y}{b}\right)X_{mn}(t) \\ &\theta_y(x,y,t) = \sum_{m=1}^{M}\sum_{n=1}^{N}\sin\left(\frac{m\pi x}{a}\right)\cos\left(\frac{n\pi y}{b}\right)Y_{mn}(t) \end{aligned} \tag{17}$$

where N and M are the truncation order. By placing the expansion in Eq. (17) into the dynamic equations and using the Galerkin method (Rezaee and Maleki 2024), also considering that the internal inertias are not effective on the amplitude of nonlinear vibrations (Rezaee et al. 2015; Minaei and

Table 1 Comparison of natural frequencies parameter, $\beta = \omega a^2\sqrt{\rho h/D}$, of a thick elastic plate using the first and third-order shear theory

h/a	Theory	1st mode	2nd mode	3rd mode
0.001	Classic theory (Leissa 1973)	11.6820	27.7526	41.1989
	First-order (Hashemi and Arsanjani 2005)	11.6815	27.7523	41.1945
	Third-order (Hosseini-Hashemi et al. 2011)	11.6815	27.7523	41.1944
	Present work	11.6815	27.7522	41.1943
0.1	3D elasticity theory (Malik and Bert 1998)	11.3984	26.2165	38.3782
	First-order (Hashemi and Arsanjani 2005)	11.3815	26.1942	38.3217
	Third-order (Hosseini-Hashemi et al. 2011)	11.3739	26.1940	38.3018
	Present work	11.3738	26.1940	38.3017
0.2	3D elasticity theory (Malik and Bert 1998)	10.7635	23.2795	32.8963
	First-order (Hashemi and Arsanjani 2005)	10.7633	23.2752	32.8428
	Third-order (Hosseini-Hashemi et al. 2011)	10.7632	23.2751	32.8427
	Present work	10.7633	23.2750	32.4226

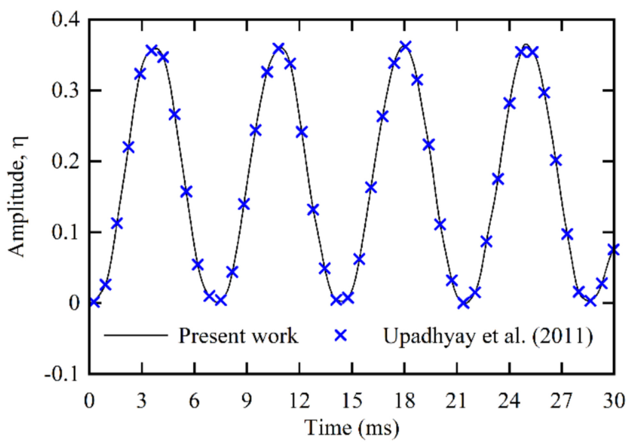

Fig. 2 Validation of the time response of fiber metal laminate plate under step loading

Arab Maleki 2020; Rezaee and Maleki 2011), nonlinear differential equations with ordinary derivatives will be obtained as following matrix form:

$$L_1W^2 + L_2W + L_3U + L_4V + L_5X + L_6Y = L_7W \tag{18a}$$

$$L_8W^2 + L_9W + L_{10}U + L_{11}V + L_{12}X + L_{13}Y = L_{14}W \tag{18b}$$

$$\begin{aligned} &L_{15}W^3 + L_{16}W^2 + L_{17}W \\ &+ L_{18}UW + L_{19}XW + L_{20}VW + L_{21}YW \\ &+ L_{22}U + L_{23}X + L_{24}V + L_{25}Y = L_{26}W \end{aligned} \tag{18c}$$

$$L_{27}U + L_{28}W^2 + L_{29}W + L_{30}X + L_{31}Y + L_{32}V = L_{33}W \tag{18d}$$

$$L_{34}U + L_{35}W^2 + L_{30}W + L_3Y + L_{38}X + L_{39}V = L_{40}W \tag{18e}$$

In Eqs. (18a–e), the coefficients L_i represent the contributions of stiffness, inertia, and foundation parameters derived from the governing equations. Coefficients L_i, $i = 1,2,\ldots,40$ derived from the series expansion of displacement components, representing the contributions of higher-order terms in the solution. These coefficients depend on material properties, geometrical constraints, border conditions, and the applied loading. Finally, by using Eqs. (18a–e) and also using the Runge–Kutta numerical technique, the above equations are solved and the nonlinear response of the system will be obtained. The nonlinear ordinary differential equations derived from Eqs. (18a–e) were solved using the fourth-order Runge–Kutta (RK4) method, implemented in MATLAB. This method provides accurate time-domain solutions by iteratively updating the system states based on the derivatives obtained from the equations (Khosravi et al. 2021). A uniform time step size $\Delta t = 10^{-6}$ s was chosen

Table 2 Material properties of fiber-metal laminate composite materials

	E_1 (GPa)	E_2 (GPa)	G_{13} (GPa)	G_{23} (GPa)	G_{12} (GPa)	ν_{12}	ρ (kg/m^3)
Composite	125.6	125.6	4.24	4.23	4.02	0.23	1872
		E (GPa)		ν			ρ (kg/m^3)
Al plate		70.5		0.32			2760

Table 3 Convergence analysis of maximum dimensionless displacement using the Galerkin method

Number of truncation order (N, M)	Maximum dimensionless displacement (center)	Change from previous term (%)
5	0.943	
8	0.989	4.88
10	1.002	1.31
12	1.003	0.1
15	1.003	0

to balance computational efficiency and accuracy. The stability of the solution was ensured by adhering to the Courant–Friedrichs–Lewy (CFL) condition, where the chosen time step size satisfies the numerical stability requirements for the system under consideration. The CFL condition ensures that the time step is sufficiently small relative to the plate's vibration frequencies. Using this approach, the nonlinear time response of the structure is computed, capturing the influence of various parameters such as the pressure pulse shape, loading duration, Pasternak foundation characteristics, aspect ratio, and laminate properties. The numerical procedure ensures the stability and convergence of the solution. For each loading case, the chosen time step provided sufficient resolution to capture the dynamic response accurately, including the effects of the loading's positive and negative phases.

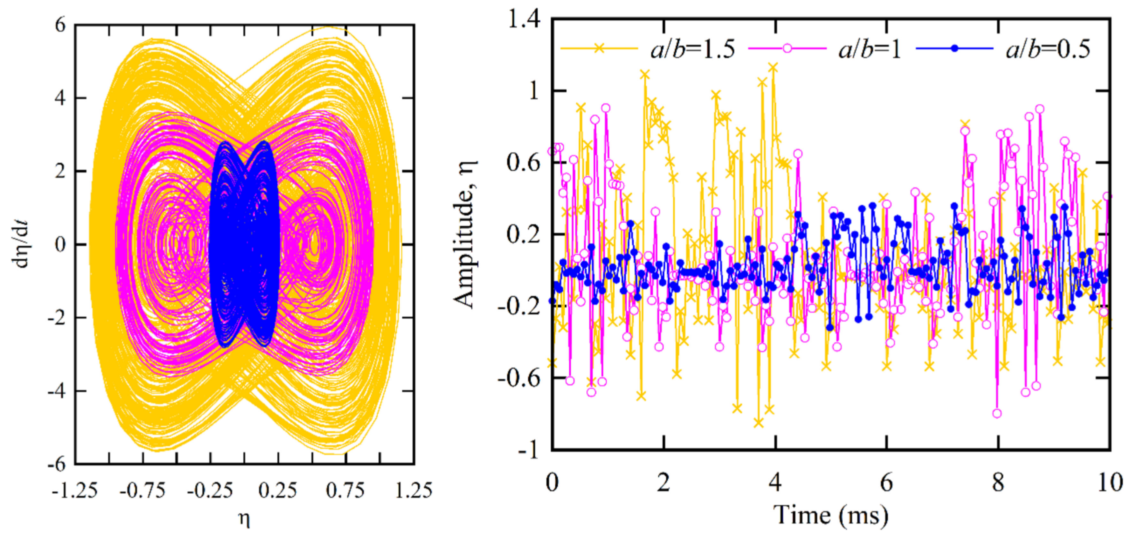

Fig. 3 Influence of aspect ratio on nonlinear time trace and phase plane under blast wave force

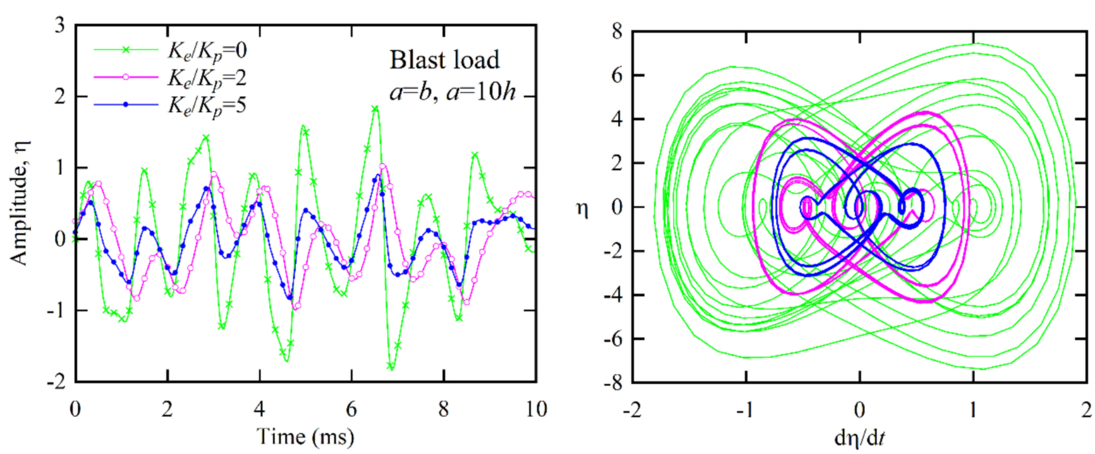

Fig. 4 Influence of the Pasternak substrate on nonlinear time response under blast wave loading

Results

In this portion, the validation of the first 3 dimensionless natural frequencies of a thick rectangular isotropic plate with simple support boundary conditions is discussed. For this purpose, first, the results obtained for a thick elastic plate are compared with the results obtained from the exact solution based on the first-order shear theory (Hashemi and Arsanjani 2005) an d the results obtained from the exact solution based on the third-order shear theory (Hosseini-Hashemi et al. 2011) in Table 1. All results presented in this study were extracted for a square plate with dimensions $a=b=20\ h$, where h is the total thickness of the plate. The thickness of the individual layers is assumed to be $h_1=h_3=0.1\ h$. The stacking sequence of the porcelain layer is defined as [Al/90/0/90/0/Al], where “Al” represents aluminum layers, and “90” and “0” indicate the orientation of the fibers in the composite layers. This specific stacking sequence and the thickness distribution are chosen to reflect typical configurations used in engineering applications and provide a consistent basis for evaluating the dynamic response under uniform pressure loading.

In another validation, the nonlinear time response of the square laminate composite FML exposed to step loading obtained by 3rd-order shear theory is compared with the results based on the 3rd-order shear model from reference (Upadhyay et al. 2011) in Fig. 2. According to Table 1 and Fig. 2, the results of the present analysis demonstrate acceptable agreement. To investigate the nonlinear dynamics of the fiber metal laminate plate under different loadings and study the effect of the effective parameters, the physical and geometrical properties of the polymer composite layers reinforced with CFRP carbon and aluminum fibers are considered as shown in Table 2.

The convergence analysis is an essential step in numerical methods, such as the Galerkin method, to ensure the accuracy and reliability of the results. This analysis evaluates how the results stabilize as amount of terms in expansion increases. The convergence analysis ensures the accurateness and reliability of results by evaluating how the solution stabilizes as the number of terms (N and M) in the Galerkin method increases. In this study, the transverse displacement $w(x,y,t)$ was calculated for $N=M=5$, 8, 10, 12, 15, using the maximum dimensionless displacement at the plate center as the reference parameter. The convergence analysis of maximum dimensionless displacement using the Galerkin technique for the case of uniform blast loading ($Q_0=100$ kPa, $t_1=0.01$ ms) is presented in Table 3. Significant changes were observed for $N=5$ and $N=8$, but at $N=10$, the results stabilized with a percentage change of only 1.31% compared to $N=8$. Further increases in N (e.g., $N=12$ and $N=15$) resulted in negligible changes ($<0.1\%$), indicating convergence. Thus, $N=M=10$ was selected for all calculations, providing an optimal balance between computational efficiency and accuracy. This analysis validates the correctness of the original results and confirms the robustness of the methodology for different types of pressure pulses.

One of the most effective factors in the behavior of plates is the aspect ratio. For this purpose, in Fig. 3, the dimensionless displacement w/h at the middle point of the plate in terms of time has been investigated. In this part, the effects of the Pasternak substrate are not considered. As

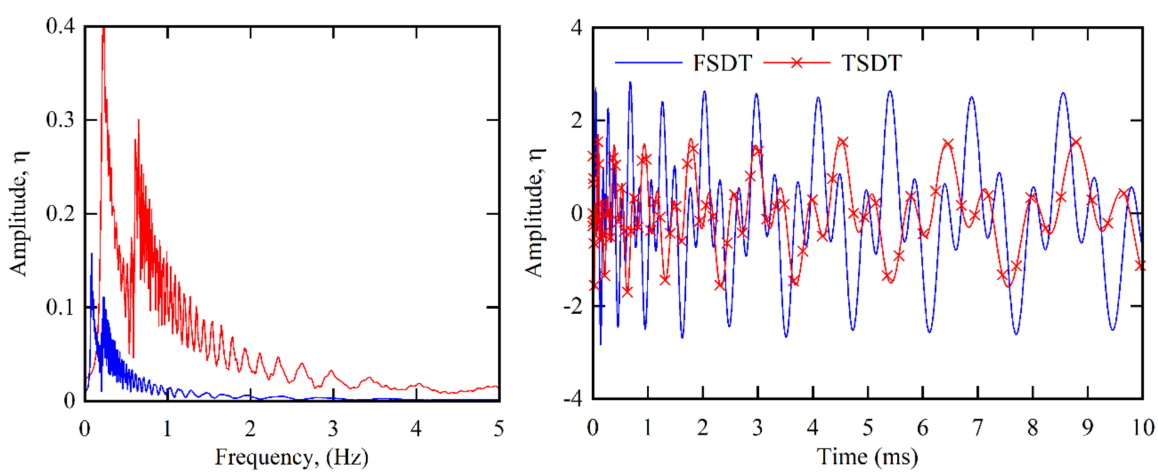

Fig. 5 Effect of first and third-order shear deformation theory displacement fields on the nonlinear time response for the displacement field

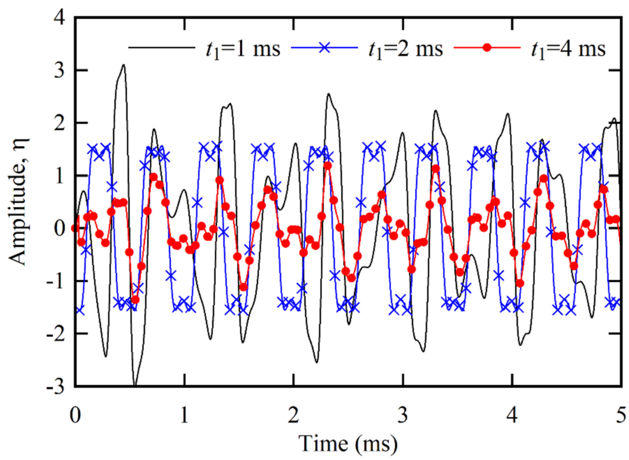

Fig. 6 Influence of duration of the positive phase of blast loading on the nonlinear time trace

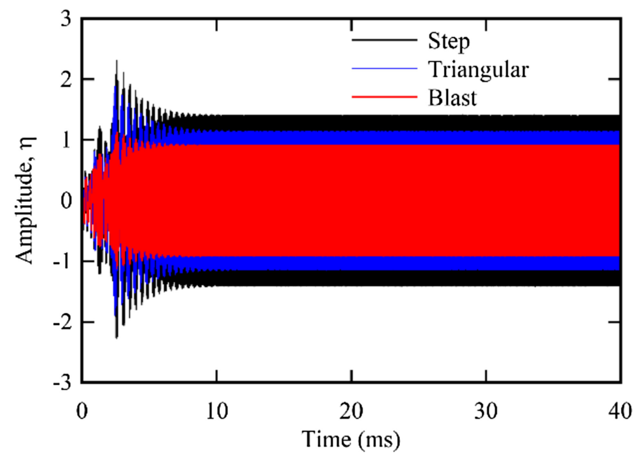

Fig. 8 Nonlinear dimensionless time response under triangular, step, and blast wave loads

can be seen, by increasing the aspect ratio from 0.4 to 1.4, the maximum dimensionless displacement has increased. Also, the frequency decreases with the increase of aspect ratio from 0.5 to 1.5. In Fig. 4, using the 3rd-order shear field, the dimensionless nonlinear time response of the fiber metal laminate has been evaluated for different values of the linear and shear stiffness of the Pasternak substrate. As can be observed, with the increase of linear and shear stiffness parameters, the oscillation amplitude decreases. It is also clear that compared to the linear stiffness constraint, the shear layer constraint has a greater influence on the time trace. In addition, it can be seen that the addition of the substrate stiffness increases the vibration frequency, and this increase is greater for the shear spring compared to the linear spring.

Figure 5 demonstrates the nonlinear time trace of fiber metal laminate under blast loading using the 3rd-order shear displacement field compared to the first-order shear displacement field. As it is clear from Fig. 5, the dimensionless time response values for the 1st-order shear theory are higher compared to the third-order shear theory. Also, the vibration frequency for the 1st-order shear theory is lower than the vibration frequency calculated based on the 3rd-order shear theory. It should be noted that with the increase in the thickness of the fiber metal laminate, the difference between the predicted values of the time response for the first and 3rd-order shear theories increases.

As observed in Fig. 5, the nonlinear responses predicted by the TSDT and FSDT show significant differences in terms of both frequency and deflection. However, in Table 1, which presents the linear natural frequencies, TSDT and FSDT produce nearly identical results. This discrepancy arises from the differences between linear and nonlinear analyses. In the linear regime (Table 1), the deflections are small, and higher-order deformation effects considered in

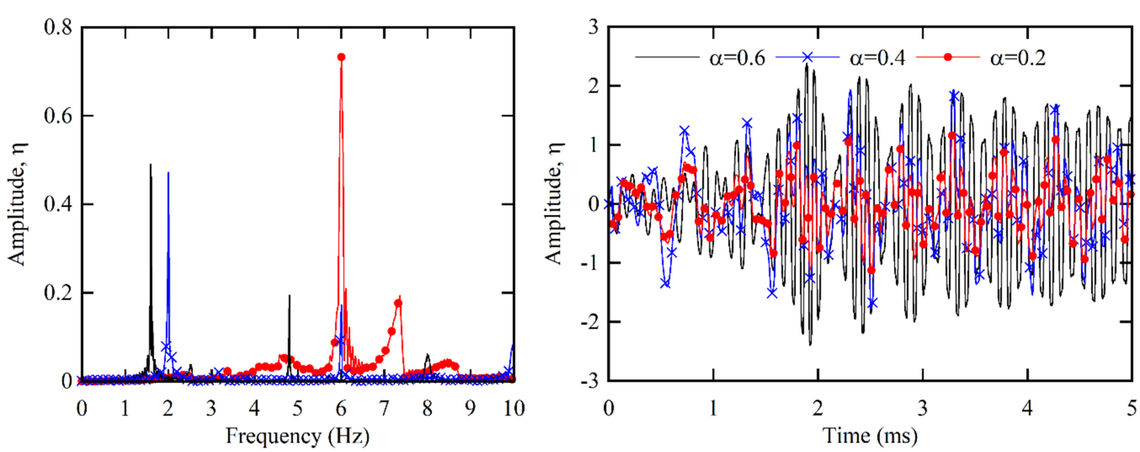

Fig. 7 Effect of blast loading wave function parameter on the nonlinear time response and frequency transform function

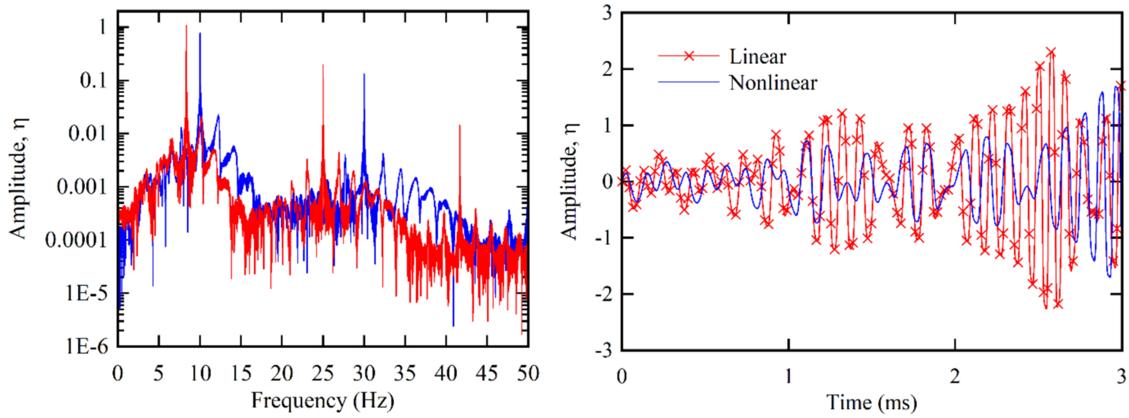

Fig. 9 Comparison of the linear and nonlinear time responses of the fiber-metal laminate plate under blast loading

TOT have minimal impact on the frequencies, leading to similar results between TSDT and FSDT. In contrast, the nonlinear response in Fig. 5 involves large deflections, where geometric nonlinearities and higher-order effects become significant. TSDT, which accounts for these effects, predicts more pronounced differences in frequency shifts and deflection amplitudes compared to FSDT, which cannot fully capture these nonlinearities. Additionally, the plate geometry and the stacking sequence amplify the differences between TSDT and FSDT in the nonlinear regime. TSDT captures the higher-order interactions between layers and shear deformations, which become prominent under large deflections, whereas FSDT oversimplifies these effects. Thus, the differences observed in Fig. 5 are attributable to the combined effects of nonlinearities, plate geometry, and composite type, which are accurately captured by TSDT but not by FSDT.

The TSDT offers significant advantages over the FSDT, particularly in scenarios involving thick plates, nonlinear behavior, and dynamic loading. Unlike FSDT, which assumes a linear variation of transverse shear stresses and requires an empirical shear correction factor, TSDT models a cubic shear stress distribution that inherently satisfies the zero shear stress boundary condition, eliminating the need for correction factors. This makes TSDT more accurate for thick plates and materials with high through-thickness property variations, such as fiber metal laminates. Additionally, TSDT is better suited for nonlinear and dynamic analyses, as it captures higher-order deformation effects that FSDT cannot, especially in cases of large deformations and complex loadings like blast waves. These benefits make TSDT a more versatile and reliable choice for advanced structural applications, where FSDT's simplifications may lead to inaccuracies.

In Fig. 6, the effects of the positive phase of blast wave loading on the nonlinear time response of the fiber metal laminate have been evaluated. As it is seen from Fig. 6, when the duration of the positive phase of blast wave loading decreases, the nonlinear time response increases, and with its increase, the negative value of the time response will grow significantly. Also, as the positive phase of loading duration increases, the frequency increases. The effects of the wave function parameter in blast loading on the nonlinear time trace of the fiber metal laminate are shown in Fig. 7. In this part, the effects of the Pasternak substrate are not considered. According to the results, by increasing the value of the wave function constraint, the influence of negative stage of the blast charging is strengthened, which indications to an growth in the displacement in the midpoint of FML. Also, increasing the value of the wave function parameter has reduced the frequencies of plate vibrations.

The influence of different loadings on the nonlinear time trace of the fiber metal laminate has been examined in Fig. 8. As can be seen, the nonlinear dimensionless time trace under step loading is greater compared to the triangular wave loading, while for triangular wave loading it is greater compared to the blast wave loading. This is because the amplitude of the oscillations is related to the loading area, which is the largest in the step loading mode and the smallest in the blast wave loading mode.

The effect of considering nonlinear strains compared to the linear case is demonstrated in Fig. 9. In this part, the effects of the Pasternak substrate are not considered. As it is known, the linear and nonlinear responses are almost similar to each other at first, but with the passage of time, their behavior becomes different from each other. According to Fig. 9, in the case of using nonlinear strains, the maximum value of the dimensionless amplitude is smaller compared to the linear case, while the frequency of the predicted vibration is larger. This frequency will also increase with the increase in the dimensionless displacement.

Conclusion

In this research, the nonlinear vibrations of the fiber metal laminate under time-dependent constant pressure loadings in the form of triangular, step, and blast waves (exponential function) have been investigated. The TSDT along with von Karman's nonlinear strain–displacement relationships are applied to obtain the nonlinear dynamic equations. The equations have been discretized using the Galerkin technique, and the time trace has been obtained using the Runge–Kutta technique. Finally, the effect of various constraints including aspect ratio, time duration of the loading positive phase, Pasternak substrate effect, and the pressure pulse type on the nonlinear time trace of the plate have been considered.

The results show that the dimensionless displacement at the center of the plate decreases exponentially with a reduction in the aspect ratio, accompanied by an increase in the frequency of plate vibrations. Furthermore, reducing the duration of the positive loading phase amplifies the amplitude of dimensionless displacement while decreasing the frequency of plate vibrations. Similarly, a decrease in the wave function parameter correlates with a reduction in the dimensionless displacement amplitude and an increase in the frequency of plate vibrations. The findings underscore the significant impact of parameters such as aspect ratio, laminate thickness, and positive loading phase duration on the structural time response. Consequently, these factors should be carefully considered during the design phase of such structures. Additionally, attention should be given to the loading time of the blast wave, as a decrease in the positive phase duration results in an amplified effect of the negative phase of the blast wave loading, potentially surpassing the frontal effect of the blast wave.

Acknowledgements This work was supported by the "Blue Project" of Jiangsu Universities (RS21QL04).

Author contributions Jin Lin: writing-original draft preparation, conceptualization, supervision, project administration.

Data availability The authors do not have permission to share data.

Declarations

Conflict of interest The author declare no competing interests.

References

Ahmadi, M., Ansari, R., Rouhi, H.: Multi-scale bending, buckling and vibration analyses of carbon fiber/carbon nanotube-reinforced polymer nanocomposite plates with various shapes. Physica E **93**, 17–25 (2017)

Amabili, M., Balasubramanian, P., Garziera, R., Royer-Carfagni, G.: Blast loads and nonlinear vibrations of laminated glass plates in an enhanced shear deformation theory. Compos. Struct. **252**, 112720 (2020)

Blala, H., Lang, L., Li, L., Alexandrov, S.: Deep drawing of fiber metal laminates using an innovative material design and manufacturing process. Compos. Commun. **23**, 100590 (2021)

Chen, Y., Yang, Y., Wang, Z., Wang, H., Li, J., Hua, L.: Accurate simulation on the forming and failure processes of fiber metal laminates: a review. Int. J. Lightweight Mate. Manuf. **6**(3), 344–356 (2023)

Costa, R.D., Sales-Contini, R.C., Silva, F.J., Sebbe, N., Jesus, A.M.: A critical review on fiber metal laminates (FML): from manufacturing to sustainable processing. Metals **13**(4), 638 (2023)

Dinh Duc, N., Tuan, N.D., Tran, P., Quan, T.Q.: Nonlinear dynamic response and vibration of imperfect shear deformable functionally graded plates subjected to blast and thermal loads. Mech. Adv. Mater. Struct. **24**(4), 318–329 (2017)

Van Do, V.N., Lee, C.-H.: Free vibration and transient analysis of advanced composite plates using a new higher-order shear and normal deformation theory. Arch. Appl. Mech. **91**, 1793–1818 (2021)

Dobyns, A.: Analysis of simply-supported orthotropic plates subject to static and dynamic loads. AIAA J. **19**(5), 642–650 (1981)

Ebrahimi, M.A., Zohoor, H., Firoozbakhsh, K., Hosseini, R.: Dynamics of a running below-knee prosthesis compared to those of a normal subject. JSM. **5**(2), 152–160 (2013)

Ebrahimi-Mamaghani, A., Koochakianfard, O., Mostoufi, N., Khodaparast, H.H.: Dynamics of spinning pipes conveying flow with internal elliptical cross-section surrounded by an external annular fluid by considering rotary inertia effects. Appl. Math. Model. **120**, 330–354 (2023)

Ebrahimi-Mamaghani, A., Koochakianfard, O., Rafiei, M., Alibeigloo, A., Dizaji, A.S., Borjalilou, V.: Machine learning, analytical, and numerical techniques for vibration analysis of submerged porous functional gradient piezoelectric microbeams with movable supports. Int. J. Struct. Stab. Dyn. (2024). https://doi.org/10.1142/S0219455426500549

Etri, H.E., Korkmaz, M.E., Gupta, M.K., Gunay, M., Xu, J.: A state-of-the-art review on mechanical characteristics of different fiber metal laminates for aerospace and structural applications. Int. J. Adv. Manuf. Technol. **123**(9), 2965–2991 (2022)

Flayyih, M.F., Hassan, T.: Predictive analytics model for students' grade prediction using machine learning. Babylon. J. Artif. Intell. **2024**, 83–101 (2024)

Gharebagh, V., Rezazadeh, G., Sharafkhani, N., Shabani, R.: Static and dynamic response of carbon nanotube-based nano-tweezers. Int. J. Eng. **24**(4), 377–386 (2011)

Gurbanov, N., Babanli, M., Turen, Y.: Metal matrix hybrid laminated composite materials. Adv. Multifunct. Lightweight Aerostruct. des. Dev. Implement. **34**(5), 73 (2020)

Hashemi, S.H., Arsanjani, M.: Exact characteristic equations for some of classical boundary conditions of vibrating moderately thick rectangular plates. Int. J. Solids Struct. **42**(3–4), 819–853 (2005)

Hoseinzadeh, M., Pilafkan, R., Maleki, V.A.: Size-dependent linear and nonlinear vibration of functionally graded CNT reinforced imperfect microplates submerged in fluid medium. Ocean Eng. **268**, 113257 (2023)

Hosseini-Hashemi, S., Fadaee, M., Taher, H.R.D.: Exact solutions for free flexural vibration of Lévy-type rectangular thick plates via third-order shear deformation plate theory. Appl. Math. Model. **35**(2), 708–727 (2011)

Hwang, W.-S., Park, H.C.: Finite element modeling of piezoelectric sensors and actuators. AIAA J. **31**(5), 930–937 (1993)

Kakati, S., Chakraborty, D.: Low velocity impact on fibre metal laminates: a review. J. Compos. Mater. **57**(30), 4731–4750 (2023)

Keshavarzian, M., Najafizadeh, M.M., Khorshidi, K., Yousefi, P., Alavi, S.M.: Non-linear free vibration analysis of a thick sandwich panel with an electrorheological core. J. Vib. Eng. Technol. **10**(4), 1495–1509 (2022)

Khosravi, S., Yousefi, M.M., Goudarzi, M.: Development of seismic fragility curves of cylindrical concrete tanks using nonlinear analysis. Amirkabir J. Civ. Eng. **53**(1), 71–88 (2021)

Leissa, A.W.: The free vibration of rectangular plates. J. Sound Vib. **31**(3), 257–293 (1973)

Lim, Y.W., Choi, H.-J., Idapalapati, S.: Design of Alporas aluminum alloy foam cored hybrid sandwich plates using Kriging optimization. Compos. Struct. **96**, 17–28 (2013)

Lu, H.: Combined forecasting schemes based on random forest regression and meta-heuristic algorithms for maximum dry density. JAISM. Bilijipub. **2**(4), 1–14 (2024)

Ma, Q., Merzuki, M., Rejab, M., Sani, M., Zhang, B.: A review of the dynamic analysis and free vibration analysis on fiber metal laminates (FMLs). Funct. Compos. Struct. **5**(1), 012003 (2023)

Madinei, H., Rezazadeh, G., Sharafkhani, N.: Study of structural noise owing to nonlinear behavior of capacitive microphones. Microelectron. J. **44**(12), 1193–1200 (2013)

Malik, M., Bert, C.W.: Three-dimensional elasticity solutions for free vibrations of rectangular plates by the differential quadrature method. Int. J. Solids Struct. **35**(3–4), 299–318 (1998)

Maraş, S., Yaman, M.: Free vibration analysis of fiber-metal laminated composite plates using differential, generalized and harmonic quadrature methods: experimental and numerical studies. Eng. Comput. **39**(6), 2326–2349 (2022)

Minaei, M., Arab Maleki, V.: Developing homotopy perturbation method to investigate the nonlinear vibration of a porous FG-beam subjected to the external excitation. J. Sci. Technol. Compos. **7**(2), 907–916 (2020)

Minaei, M., Rezaee, M., Arab Maleki, V.: Vibration analysis of viscoelastic carbon nanotube under electromagnetic fields based on the nonlocal Timoshenko beam theory. Iran. J. Mech. Eng. Trans. ISME **23**(2), 176–198 (2021)

Nasrabadi, M., Sevbitov, A.V., Maleki, V.A., Akbar, N., Javanshir, I.: Passive fluid-induced vibration control of viscoelastic cylinder using nonlinear energy sink. Mar. Struct. **81**, 103116 (2022)

Ng, L.F., Yahya, M.Y., Leong, H.Y., Parameswaranpillai, J., Muthukumar, C., Syed Hamzah, S.M.S.A., Dhar Malingam, S.: State-of-the-art review on developing lightweight fiber-metal laminates based on synthetic/natural fibers. Polym. Compos. **44**(10), 6275–6303 (2023)

Niu, Y., Abdalla, I.H., Jabur, Yk., Jassim, S.A., Mohammed, Mk., Sulaiman, B.H., Alsultan, Q.H., deen Shawqi, O.S.A., Mohameed, Oj., Abed, T.H., Panessai, I.Y.P., Khalaf, H.A.K., Abdulbaqi, A.S.A., Jia, Z.J., Wang, H., Abdulrahman, M.M., Nejrs, S.M.: Development of high-effectiveness photocatalytic materials for water purification and environmental remediation. Khwarizmia **2023**, 84–94 (2023)

Patel, M., Patel, S., Ahmad, S.: Blast analysis of efficient honeycomb sandwich structures with CFRP/Steel FML skins. Int. J. Impact Eng **178**, 104609 (2023)

Pourreza, T., Alijani, A., Maleki, V.A., Kazemi, A.: Nonlinear vibration of nanosheets subjected to electromagnetic fields and electrical current. Adv. Nano Res. **10**(5), 481–491 (2021)

Pourreza, T., Alijani, A., Maleki, V.A., Kazemi, A.: The effect of magnetic field on buckling and nonlinear vibrations of graphene nanosheets based on nonlocal elasticity theory. Int. J. Nano Dimens. **13**(1), 54–70 (2022)

Pourreza, T., Alijani, A., Maleki, V.A., Kazemi, A.: Nonlinear vibrations of graphene nanoplates with arbitrarily orientated crack located in magnetic field using nonlocal elasticity theory. Int. J. Struct. Integr. (2025). https://doi.org/10.1108/IJSI-10-2024-0178

Rao, S.S.: Vibration of Continuous Systems. Wiley, Hoboken (2019)

Reddy, J.N.: Mechanics of Laminated Composite Plates and Shells: Theory and Analysis. CRC Press, Boca Raton (2003)

Rezaee, M., Maleki, V.: A new nonlinear model for flexural vibration analysis of a cracked beam with a fatigue crack. J. Appl. Comput. Sci. Mech. **22**(2), 35–52 (2011)

Rezaee, M., Maleki, V.A.: On the complex mode shapes and natural frequencies of clamped-clamped fluid-conveying pipe. Appl. Ocean Res. **150**, 104113 (2024)

Rezaee, M., Sharafkhani, N.: Nonlinear dynamic analysis of an electrostatically actuated cylindrical micro-beam subjected to cross fluid flow. Int. J. Appl. Mech. **11**(06), 1950061 (2019)

Rezaee, M., Javadian, H., Maleki, V.A.: Vibration behavior and crack detection of a cracked short beam under a axial load. Mech. Eng. **47**(2), 1–4 (2015)

Rezaee, M., Fathi, R., Maleki, V.A.: Dynamic analysis and uncertainty modeling of viscoelastic beam response to fluid stimulation: insights into nonlinear effects and velocity uncertainties. Appl. Ocean Res. **157**, 104487 (2025)

Samuel, C., Adewunmi, D.: Enhancing undrained shear strength prediction through innovative hybridization techniques. J. Artif. Intell. Syst. Model. **1**(02), 1–14 (2024)

Shabani, R., Sharafkhani, N., Tariverdilo, S., Rezazadeh, G.: Dynamic analysis of an electrostatically actuated circular micro-plate interacting with compressible fluid. Acta Mech. **224**, 2025–2035 (2013)

Sharafkhani, N., Orwa, J.O., Adams, S.D., Long, J.M., Lissorgues, G., Rousseau, L., Kouzani, A.Z.: An intracortical polyimide microprobe with piezoelectric-based stiffness control. J. Appl. Mech. **89**(9), 091008 (2022)

Shooshtari, A., Razavi, S.: A closed form solution for linear and nonlinear free vibrations of composite and fiber metal laminated rectangular plates. Compos. Struct. **92**(11), 2663–2675 (2010)

Smolnicki, M., Lesiuk, G., Duda, S., de Jesus, A.: A review on finite-element simulation of fibre metal laminates. Arch. Comput. Methods Eng. **30**(2), 749–763 (2023)

Szekrenyes, A.: Application of differential quadrature method to delaminated first-order shear deformable composite plates. Thin-Walled Struct. **166**, 108028 (2021)

Upadhyay, A., Pandey, R., Shukla, K.: Nonlinear dynamic response of laminated composite plates subjected to pulse loading. Commun. Nonlinear Sci. Numer. Simul. **16**(11), 4530–4544 (2011)

Wang, Z., Zhang, X., Liu, M., Zhou, Y., Zha, Z., Li, C., Yang, Y., Wang, J., Jiang, F.: Microstructure characterization and mechanical properties of the 304SS-(NiTif/FeAl) metal-intermetallic laminate composites. J. Alloys Compd. **943**, 169117 (2023)

Xie, M., Zhan, L., Ma, B., Hui, S.: Classification of fiber metal laminates (FMLs), adhesion theories and methods for improving interfacial adhesion: a review. Thin-Walled Struct. **198**, 111744 (2024)

Zhao, L., Wang, M., Yang, R., Zhao, M., Song, Z., Bohlooli, N.: Using three-dimensional theory of elasticity for vibration analysis of laminated sectorial plates. Steel Compos. Struct. **48**(1), 1–17 (2023)

Zhen, W., Rui, M., Yongzhi, L., Yushan, X., Jie, M.: An advanced five-unknown higher-order theory for free vibration of composite and sandwich plates. Chin. J. Aeronaut. **34**(9), 104–118 (2021)